Research Square

Preprints are preliminary reports that have not undergone peer review.
They should not be considered conclusive, used to inform clinical practice,
or referenced by the media as validated information.

Effects of Zn addition on the microstructure and corrosion behavior of as-extruded Mg–Al–Ca–Mn-based alloys

Yongping Zheng
Zhejiang University of Technology
Jie Xu
Zhe Jiang Taotao Vehicles CO., LTD
Xuanbing Wang
Zhejiang Kehon Intelligent Science & Technology CO.LTD
Guofu Zou
Zhe Jiang Taotao Vehicles CO., LTD
Leipeng Song
124018@zust.edu.cn
Zhejiang University of Technology

Article

Keywords: Mg–Al–Ca–Mn alloy, Zn addition, Microstructure, Corrosion behavior

Posted Date: November 2nd, 2026

DOI: https://doi.org/10.21203/rs.3.rs-11342739/v1

License: This work is licensed under a Creative Commons Attribution 4.0 International License.
Read Full License

Additional Declarations: No competing interests reported.

Effects of Zn addition on the microstructure and corrosion behavior of as-extruded Mg–Al–Ca–Mn-based alloys

Abstract The influence of Zn addition (0–0.6 wt.%) on the microstructure and the corrosion behavior of as-extruded Mg–1Al–0.3Ca–0.3Mn (wt.%) alloys was investigated by X-ray diffraction, optical microscopy, scanning electron microscopy combined with energy-dispersive X-ray spectroscopy, immersion tests and electrochemical measurements in 3.5 wt.% NaCl solution. All the as-extruded alloys consist of an α-Mg matrix and a small fraction of Al_4Ca particles distributed along the grain boundaries; no Zn-bearing phase is detected over the composition range studied, so that Zn is retained in solid solution. Immersion tests show that a small Zn addition markedly improves the corrosion resistance: after 168 h the corrosion rate of the alloy containing 0.2 wt.% Zn is 4.77×10^{-4} g cm^{-2} h^{-1}, which is only 14.3% of that of the Zn-free alloy. Potentiodynamic polarization confirms the same ranking, the corrosion potential shifting from −1.490 V to −1.440 V and the corrosion current density decreasing from 71.1 μA cm^{-2} to 15.4 μA cm^{-2}. Electrochemical impedance spectroscopy, however, ranks the four alloys differently. Because the grain-size sequence does not track the corrosion-rate sequence—the alloy with the finest grains does not exhibit the lowest corrosion rate—grain refinement alone cannot account for the observed improvement. The beneficial effect is instead attributed to Zn dissolved in the α-Mg matrix, which modifies the growth of the corrosion-product film and limits the area over which micro-galvanic coupling at the Al_4Ca particles can operate; this effect is optimal at 0.2 wt.% Zn and is weakened when a higher Zn content coarsens the grains.

Keywords Mg–Al–Ca–Mn alloy; Zn addition; Microstructure; Corrosion behavior;

1 Introduction

Magnesium alloys are the lightest metallic structural materials and offer a high specific strength, a low density, good machinability and excellent recyclability, which makes them attractive for reducing the weight of automotive and aerospace components [1–3]. Their widespread use is nevertheless still restricted by a poor corrosion resistance. The standard electrode potential of magnesium is very negative, and the hydroxide film that forms spontaneously in aqueous media is only partially protective, so that in chloride-containing environments the matrix dissolves readily and localized attack develops [4,5]. Closing the gap between the mechanical potential of magnesium alloys and their service performance therefore requires a systematic improvement of their corrosion resistance rather than a further optimization of strength alone.

Alloying is the most practical route to improve the corrosion behavior of magnesium alloys, and it operates through two complementary effects: a shift of the corrosion potential and a change in the compactness and the stability of the surface film [6,7]. Surface modification and coating technologies offer an alternative route, but they add processing steps and cost [8]. The elements most frequently used for alloying purposes are Al, Zn, Mn, Ca, Zr and the rare-earth (RE) elements

[9–13]. For instance, extruded Mg–8Sn–1Zn alloys containing less than 0.3 wt.% Al have been reported to exhibit an excellent corrosion resistance [14], whereas Baek et al. [15] demonstrated that the corrosion resistance of extruded AZ61 alloy is improved by the addition of 0.1–0.5 wt.% Ca. In the same alloy family, the corrosion rates of extruded Mg–6Al–1Zn–0.5Ca–0.3Mn (wt.%) alloys were reported to be about six times higher than those of the corresponding alloys containing 0.25 wt.% Y [16]. These results show that the response of a magnesium alloy to a given alloying element depends strongly on the base composition, which makes a case-by-case assessment necessary.

Among the possible additions, Zn deserves particular attention because it is inexpensive, it is tolerated as an impurity in commercial magnesium alloys [3,17], and it influences both the mechanical properties and the corrosion behavior. The reported effects of Zn on corrosion are, however, contradictory. The corrosion rate of binary Mg–Zn alloys has been reported to increase and then decrease with increasing Zn content, as a result of the interplay between the amount of second phase and the resulting galvanic coupling [18]. In contrast, Yan et al. [19] found that the corrosion potential of extruded Mg–Zn alloys decreases while the corrosion current density increases as the Zn concentration is raised, that is, that Zn is detrimental under those conditions. Zhang et al. [20] reported that the addition of 0.6 wt.% Zn to a magnesium matrix improves the corrosion resistance, and the addition of 1.6 wt.% Zn to an Mg–0.6Si alloy has been shown to improve both the mechanical and the corrosion properties [21]. A systematic study of binary Mg–X alloys in chloride media likewise showed that the effect of Zn on the corrosion rate is small compared with that of elements such as Fe, Ni and Cu, but not negligible [22]. Because the sign and the magnitude of the Zn effect depend on the amount of Zn that remains in solid solution, on the nature and the volume fraction of the second phases that form, and on the corrosion medium, an optimum Zn content cannot be transferred from one alloy system to another.

Extruded Mg–Al–Ca–Mn-based alloys have recently attracted considerable interest because they combine a high strength with a low cost and do not rely on rare-earth additions [23–25]. Their microstructure and their mechanical behavior have been studied in some detail in the dilute regime [26]. Dilute Mg–Al–Ca–Mn alloys with a low Al content are also of interest because they avoid the coarse Al–Ca phases that act as strong cathodic sites at higher Al contents [27]. In contrast, the corrosion behavior of these dilute alloys has been examined only recently, and the specific role played by Zn in them remains unclear. In particular, it is not known whether the small Zn additions that are effective in other magnesium systems retain their beneficial effect in a dilute Mg–Al–Ca–Mn matrix, in which almost all of the Zn can be accommodated in solid solution and in which the only second phase present is a small fraction of Al_4Ca.

In the present investigation, Mg–1Al–0.3Ca–0.3Mn-based alloys with Zn contents of 0, 0.2, 0.4 and 0.6 wt.% were subjected to indirect extrusion, and the influence of the Zn addition on the microstructure and on the corrosion behavior in 3.5 wt.% NaCl solution was studied systematically by immersion tests, potentiodynamic polarization and electrochemical impedance spectroscopy (EIS). The results show that the addition of 0.2 wt.% Zn improves the corrosion resistance markedly, that the improvement is not controlled by grain size, and that EIS performed shortly after immersion does not reproduce the ranking obtained by mass loss. The origin of these observations

is discussed in terms of the distribution of Zn between the matrix and the grain boundaries, of the micro-galvanic coupling at the Al4Ca particles, and of the time scale over which each technique probes the corroding interface.

2 Experimental Part

Mg–1Al–0.3Ca–0.3Mn-based (wt.%) alloys with different Zn contents were prepared from high-purity Mg, Al and Zn (≥99.9%) and from Mg–20 wt.% Ca and Mg–5 wt.% Mn master alloys in a vacuum induction furnace under an argon atmosphere. The nominal compositions of the four alloys are listed in Table 1; according to their nominal Zn content they are denoted ACMZ0, ACMZ2, ACMZ4 and ACMZ6, respectively.

Table1 The compositions (wt%) of the studied alloys.

Alloys	Nominal composition	Al	Ca	Mn	Zn	Mg
ACMZ0	Mg-1Al-0.3Ca-0.3Mn	1	0.3	0.3	0	Bal.
ACMZ2	Mg-1Al-0.3Ca-0.3Mn-0.2Zn	1	0.3	0.3	0.2	Bal.
ACMZ4	Mg-1Al-0.3Ca-0.3Mn-0.4Zn	1	0.3	0.3	0.4	Bal.
ACMZ6	Mg-1Al-0.3Ca-0.3Mn-0.6Zn	1	0.3	0.3	0.6	Bal.

The cylindrical cast billets (Φ40 mm × 45 mm) were homogenized at 410 °C for 24 h and then water-quenched. The homogenized billets were subsequently indirect-extruded at 275 °C with an extrusion ratio of 9:1. The phase constituents of the as-cast alloys were identified by X-ray diffraction (XRD) on an X'Pert diffractometer. The microstructure was characterized parallel to the extrusion direction (ED) using an MR5000 optical microscope (OM) and a JSM-6360CA scanning electron microscope (SEM, JEOL) equipped with an Oxford energy-dispersive X-ray spectrometer (EDS).

The corrosion behavior of the as-extruded specimens was evaluated by immersion tests and by electrochemical measurements. For the immersion tests, cylindrical specimens of Φ13 mm × 2 mm were mechanically ground with SiC paper up to 7000 grit, ultrasonically cleaned in pure ethanol and dried. The specimens were then immersed in 3.5 wt.% NaCl solution at room temperature for 24, 48, 72, 96, 120, 144 and 168 h. After immersion, the specimens were cleaned for 3 min in a 180 g L^{-1} CrO_3 solution to remove the corrosion products and were then ultrasonically cleaned and dried. The surface morphology of the corroded specimens was examined by SEM. The mass loss of each specimen was measured, and the corrosion rate was calculated as

$$v = (w_1 - w_2) / (A\ t) \quad (1)$$

where v is the corrosion rate (g cm^{-2} h^{-1}), w_1 is the mass of the specimen before immersion (g), w_2 is the mass after immersion and after removal of the corrosion products (g), A is the exposed area of the specimen (cm^2) and t is the immersion time (h).

Electrochemical measurements were carried out on a Reference 3000 electrochemical workstation using a conventional three-electrode cell with a saturated calomel electrode (SCE) as the reference electrode, a platinum plate as the counter electrode and the specimen as the working

electrode. Potentiodynamic polarization curves were recorded in 3.5 wt.% NaCl solution at room temperature on specimens with an exposed area of 1 cm^2, using a scan rate of 1 mV s^{-1} over a potential range from −0.4 V to 0.4 V with respect to the open-circuit potential. The corrosion potential (Ecorr) and the corrosion current density (icorr) were obtained by Tafel extrapolation. Electrochemical impedance spectra were acquired at the open-circuit potential after an initial stabilization period of 120 s, over a frequency range from 10^{-2} to 10^4 Hz.

3 Results

3.1 Microstructure

Fig. 1 shows the XRD patterns of the as-cast Mg–Al–Ca–Mn-based alloys with different Zn contents. The main phases present in all four alloys are α-Mg and Al_4Ca. The positions and the relative intensities of the α-Mg and Al4Ca peaks are essentially the same for the alloys with and without Zn, and no peak that could be assigned to a Zn-bearing phase is observed. This is consistent with the composition of the alloys: the maximum solid solubility of Zn in α-Mg is far above 0.6 wt.% at the homogenization temperature, so that all of the Zn added here is expected to remain in solid solution. It is also worth noting that the overall atomic ratio of Al to Ca in the present alloys (≈4.9) is higher than the stoichiometric value of Al4Ca, which means that Al_4Ca is the equilibrium Al–Ca phase and that the excess Al is retained in the α-Mg matrix. The broadening of the diffraction peaks that has been reported for refined microstructures and for cold-deformed structures with a high stored energy is not observed here [17].

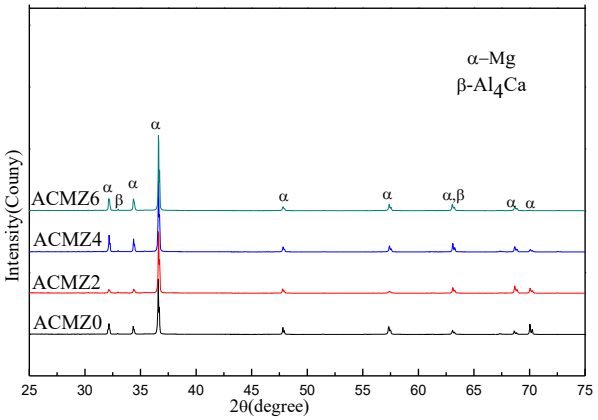


Fig.1. XRD patterns of as-cast Mg-1Al-0.3Ca-0.3Mn-based alloys.

Fig. 2 shows optical micrographs of the as-extruded alloys with different Zn contents. The microstructures consist mainly of fine equiaxed grains together with a few coarse elongated grains, indicating that dynamic recrystallization (DRX) did not proceed to completion in any of the extruded alloys. The average grain sizes were measured to be 6.12, 5.46, 5.14 and 7.03 μm for the ACMZ0, ACMZ2, ACMZ4 and ACMZ6 alloys, respectively. The average grain size therefore decreases as long as the Zn content is below 0.4 wt.% and then increases as the Zn content is raised further.

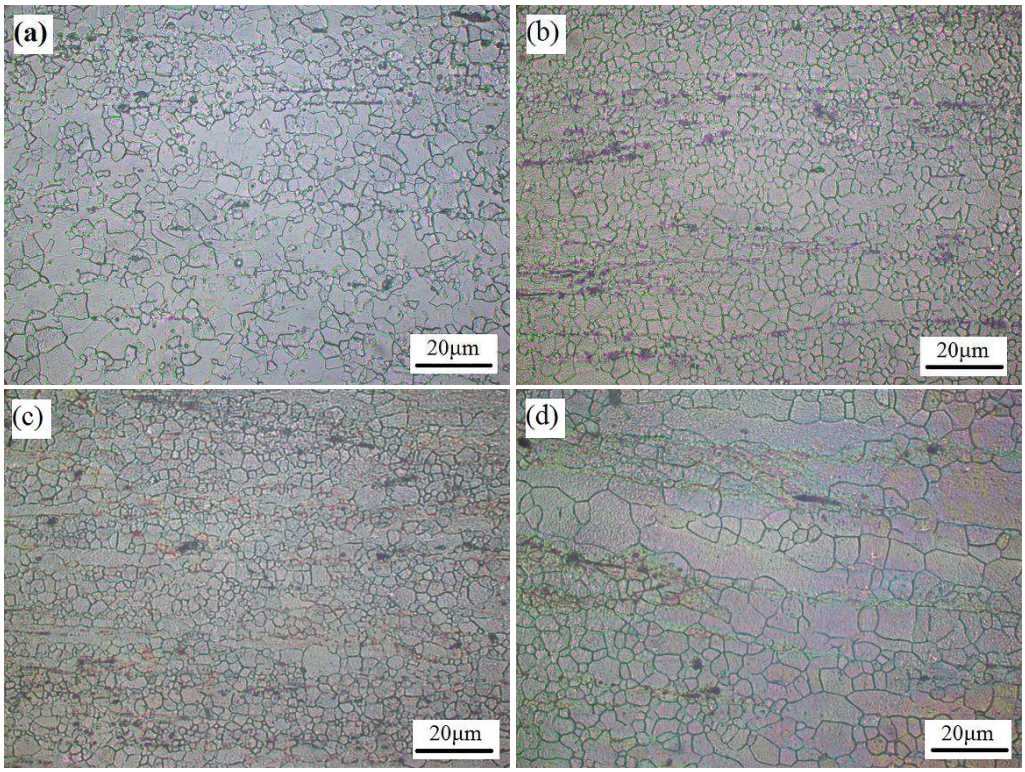
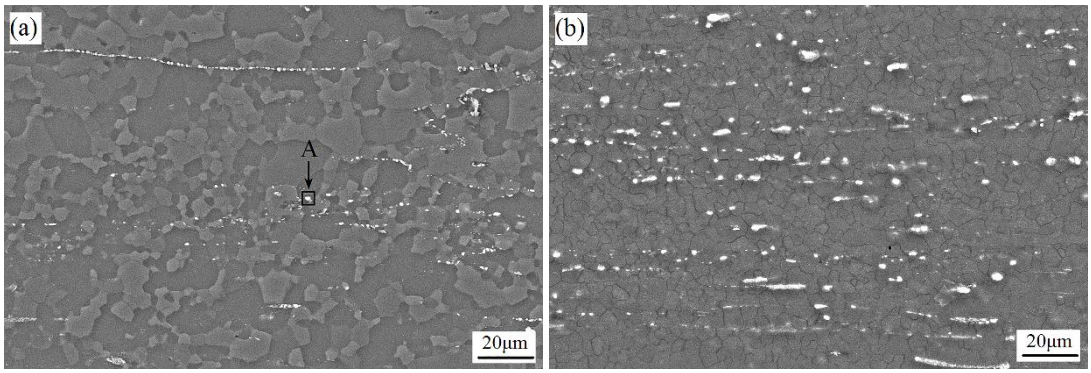


Fig.2. Optical micrographs of as-extruded Mg-1Al-0.3Ca-0.3Mn-based alloys: (a) ACMZ0; (b) ACMZ2; (c) ACMZ4; (d) ACMZ6.

Fig. 3a–e show SEM micrographs of the as-extruded alloys and the EDS analysis of the second phase in the ACMZ0 alloy at the position marked A. Taken together with the XRD results in Fig. 1, these observations demonstrate that Al_4Ca is the dominant intermetallic phase and that it is distributed along the grain boundaries. EDS analysis of the particle marked A gives 72.6 wt.% Mg, 19.3 wt.% Al and 8.1 wt.% Ca. The absolute values are influenced by the surrounding α-Mg matrix because the particles are smaller than the EDS interaction volume, but the corresponding Al/Ca atomic ratio (≈ 3.5) is consistent with the Al_4Ca stoichiometry identified by XRD. In addition, the Al4Ca particles are broken up during extrusion and form stringers aligned along the extrusion direction.



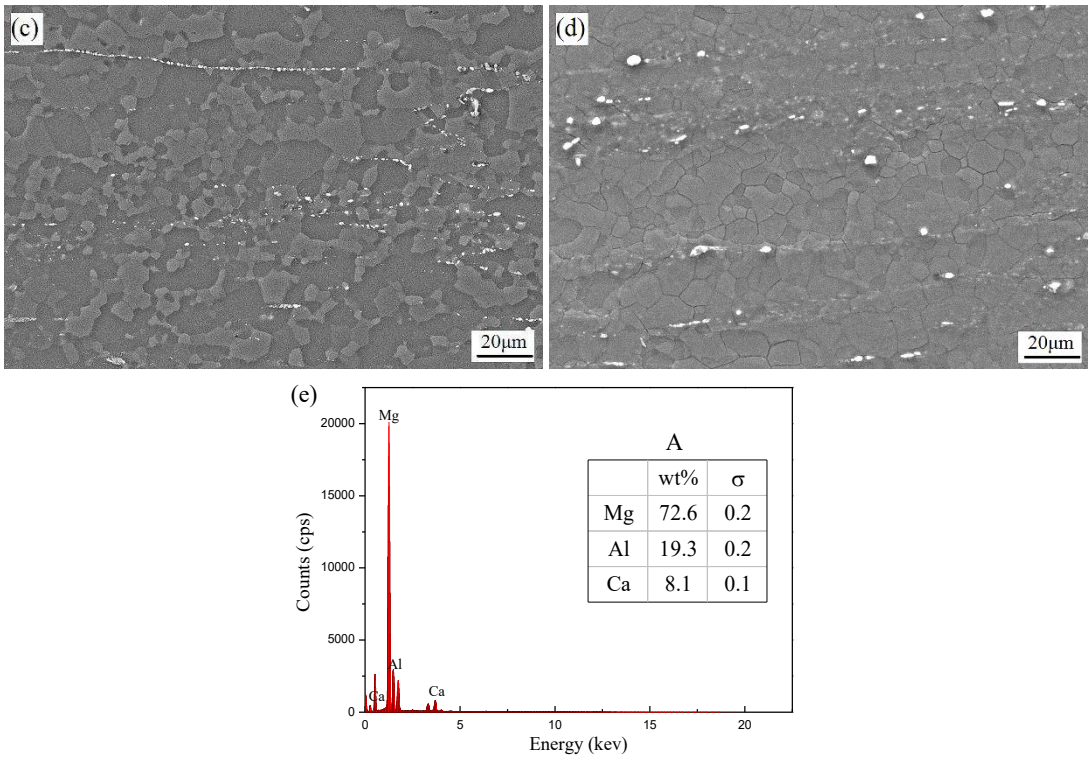


Fig.3. SEM micrographs of as-extruded Mg-1Al-0.3Ca-0.3Mn-based alloys: (a) ACMZ0; (b) ACMZ2; (c) ACMZ4; (d) ACMZ6; (e) EDS analysis of the second phase in ACMZ0 corresponding to assigned A region

3.2 Immersion tests

Fig. 4 shows the macroscopic appearance, with the corrosion products retained, of the as-extruded alloys after immersion for different times. During immersion, gas bubbles adhered to the specimen surfaces and the solution became progressively turbid as a result of the formation and the detachment of corrosion products. The ACMZ0 specimens were corroded more severely than the other alloys, and localized corrosion with deep pits was already evident after 24 h of immersion. The addition of Zn therefore improves the corrosion resistance of the as-extruded ACMZ0 alloy, and the improvement achieved with 0.2 wt.% Zn is particularly pronounced: the ACMZ2 specimens remained comparatively smooth and retained a metallic appearance up to 168 h, whereas the ACMZ0 and ACMZ4 specimens became covered by a thick, partly detached corrosion-product layer.

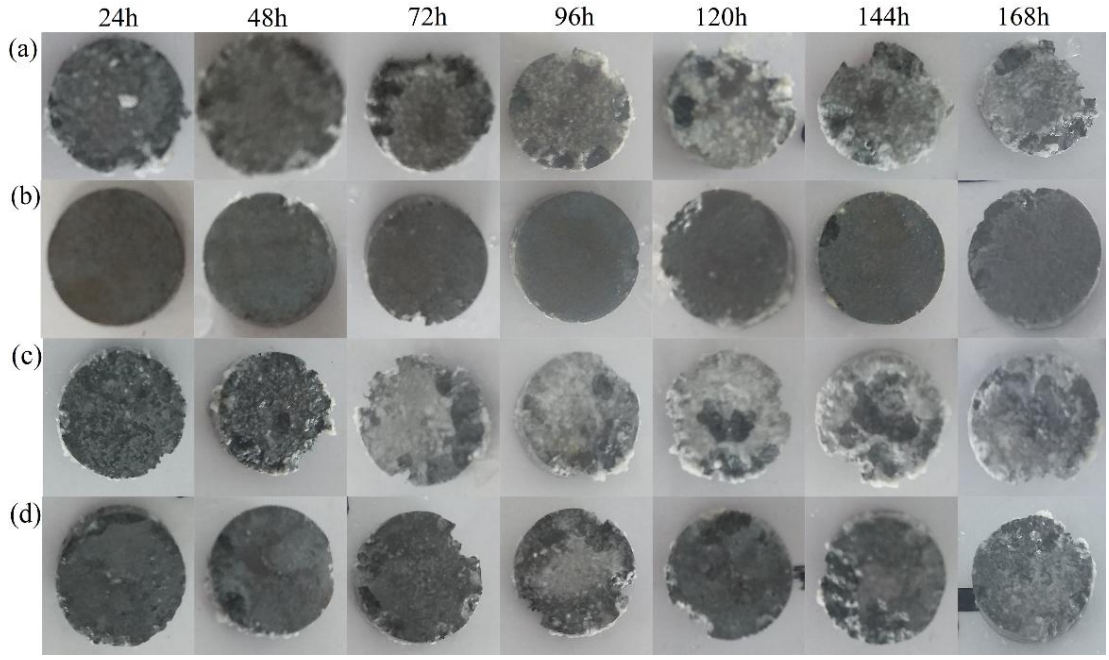


Fig.4. Optical micrographs showing the macroscopic surface of as-extruded Mg-1Al-0.3Ca-0.3Mn-based alloys: (a) ACMZ0; (b) ACMZ2; (c) ACMZ4; (d) ACMZ6.

Fig. 5 shows the surface microtopography of the ACMZ2 alloy after removal of the corrosion products for different immersion times. Pitting corrosion is the dominant corrosion mode of the ACMZ2 alloy throughout the immersion period. After 24 h of immersion the corrosion pits are about 1–3 μm in size; after 168 h the specimen surface is entirely covered by pits and the pit size has increased to about 10–15 μm.

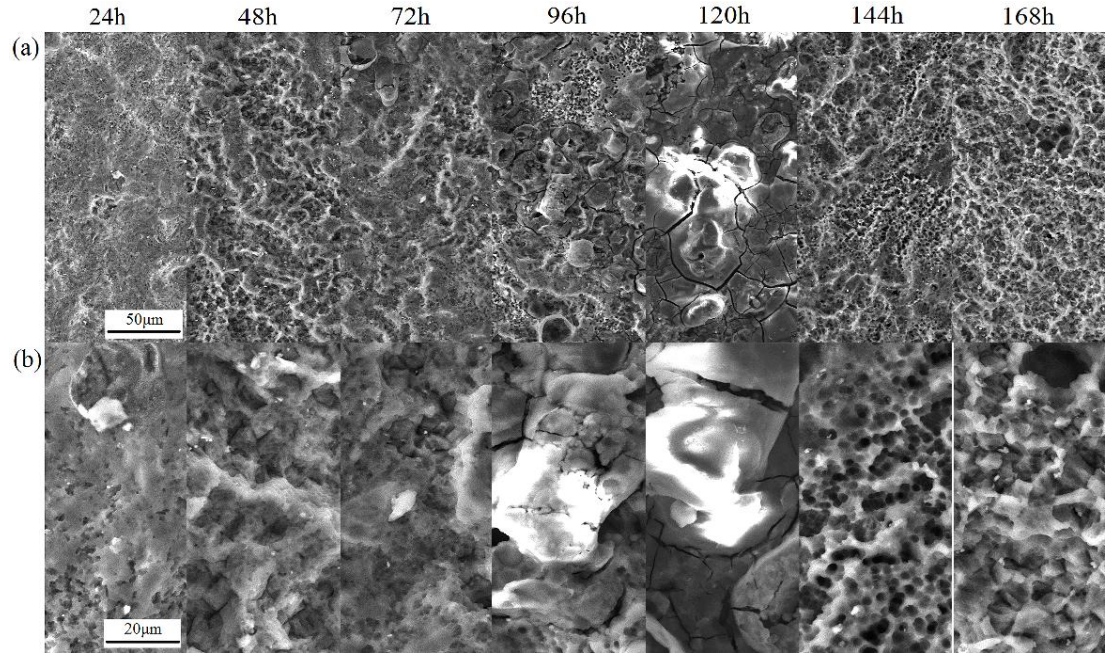
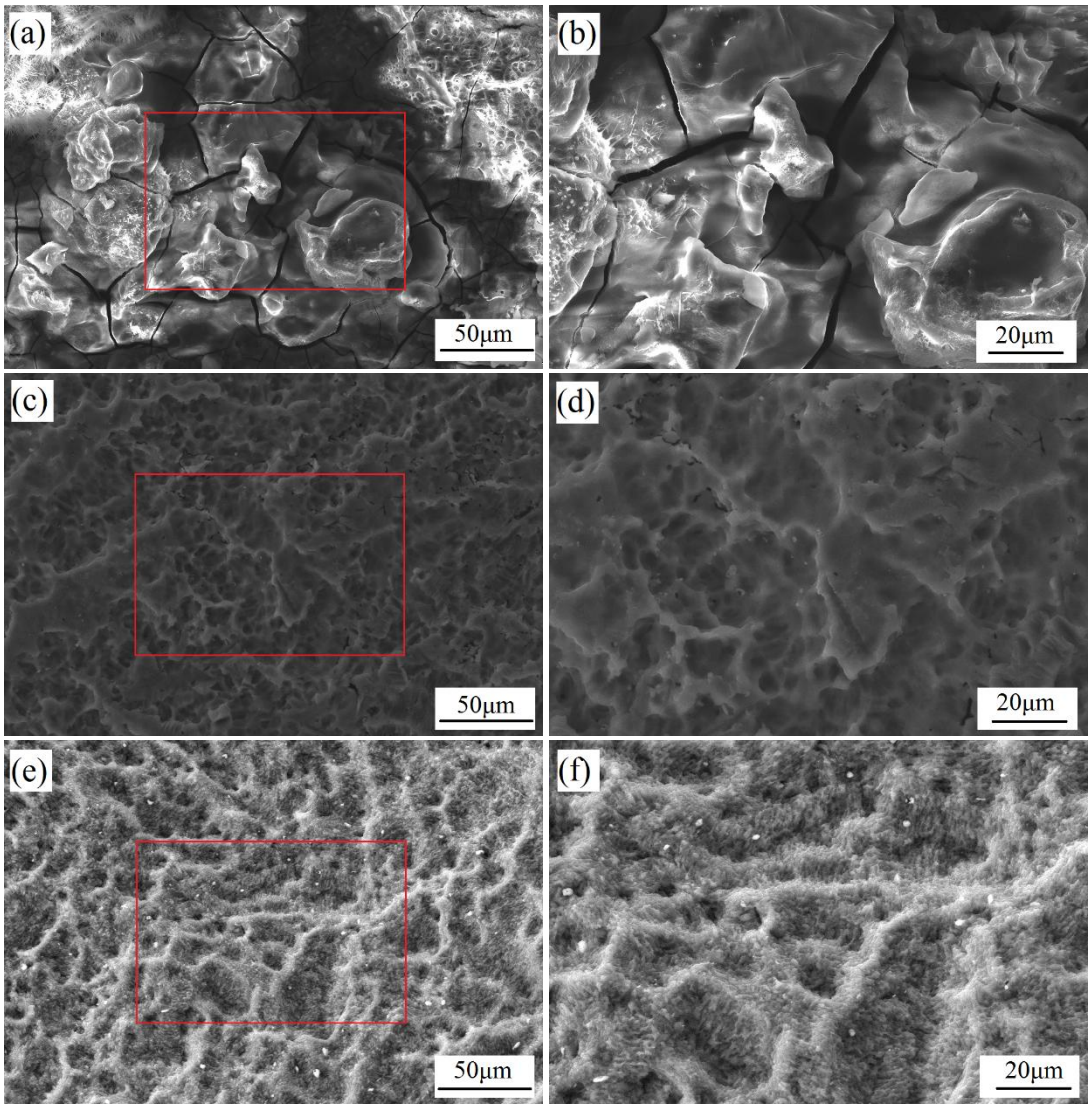


Fig.5. Microtopography of ACMZ2 alloy with different immersion time: (a) low magnification; (b) high magnification.

The SEM micrographs in Fig. 6 show the corroded surfaces of the as-extruded alloys after removal of the corrosion products following 168 h of immersion. Cracks, which provide pathways for Cl^- ions to enter the magnesium matrix, are present in the ACMZ0 alloy (Fig. 6a and b). Arrays of deep pits are superimposed on the surface of all the Zn-containing alloys (Fig. 6c–h), which indicates that localized corrosion took place throughout the immersion process. It is notable that the ACMZ2 alloy exhibits the least severe pitting of the four alloys, which confirms its superior corrosion resistance.



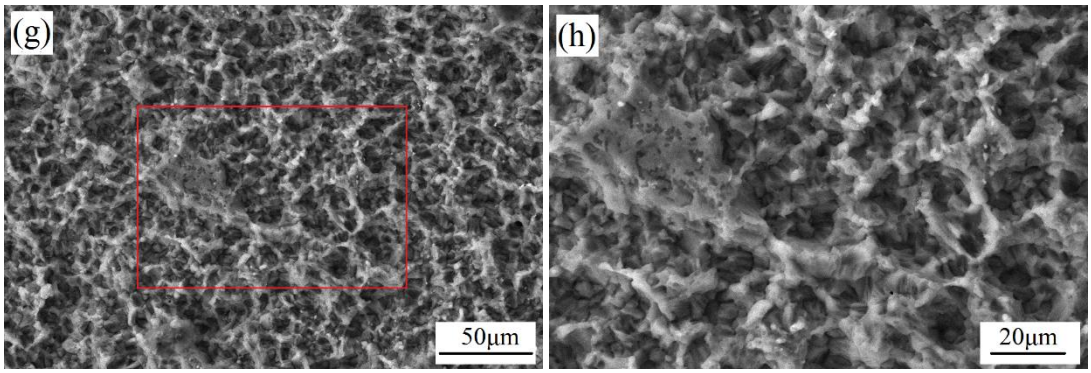


Fig.6. SEM micrographs of corroded appearance (after removal of corrosion product) after 168h immersion for as-extruded Mg-1Al-0.3Ca-0.3Mn-based alloys: (a, b) ACMZ0; (c, d) ACMZ2; (e, f) ACMZ4; (g, h) ACMZ6; (a, c, e, g) low magnification; (b, d, f, h) high magnification.

Fig. 7 summarizes the mass losses and the corrosion rates of the as-extruded alloys as a function of immersion time. The corrosion rate decreases as the immersion time increases. This behavior can be understood in terms of the successive stages of the corrosion process: at the beginning of the immersion, the large contact area between the alloy matrix and the solution leads to a high corrosion rate; at intermediate times, the corrosion products that accumulate on the specimen surface partially block the active sites and lower the rate; at longer times, the corrosion products build up into a layer that restricts the access of Cl^- ions to the α-Mg matrix, so that the corrosion reaction becomes relatively stable and the corrosion rate approaches a plateau. The corrosion rates after 168 h of immersion were measured to be 3.34×10^{-3}, 4.77×10^{-4}, 3.01×10^{-3} and 1.54×10^{-3} g cm^{-2} h^{-1} for the ACMZ0, ACMZ2, ACMZ4 and ACMZ6 alloys, respectively. When the Zn content reaches 0.2 wt.%, the corrosion rate after 168 h of immersion is 4.77×10^{-4} g cm^{-2} h^{-1}, which is only 14.3% of that of the ACMZ0 alloy. The corrosion rate of the ACMZ2 alloy is therefore significantly lower than that of the other three alloys.

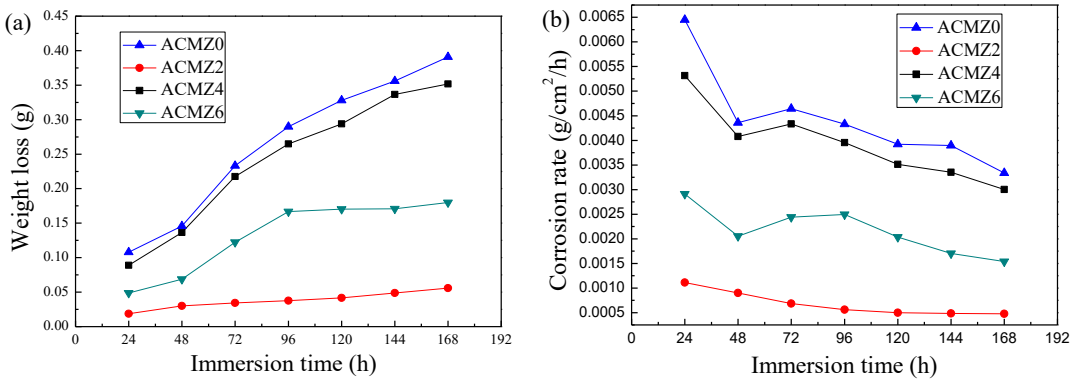


Fig.7. Weight losses and corrosion rate of as-extruded Mg-1Al-0.3Ca-0.3Mn-based alloys: (a) weight loss; (b) corrosion rate.

3.3 Electrochemical measurements

Fig. 8 shows the potentiodynamic polarization curves of the as-extruded alloys. Each curve consists of a cathodic branch on the left-hand side and an anodic branch on the right-hand side, and all four curves follow Tafel behavior. No passivation is observed, which indicates that the protective layer formed by the corrosion products cannot provide a durable and effective protection

for the magnesium matrix. The cathodic branches of the four alloys almost coincide, which shows that the Zn addition has only a slight influence on the cathodic reduction reaction, whereas it has a pronounced influence on the anodic reaction.

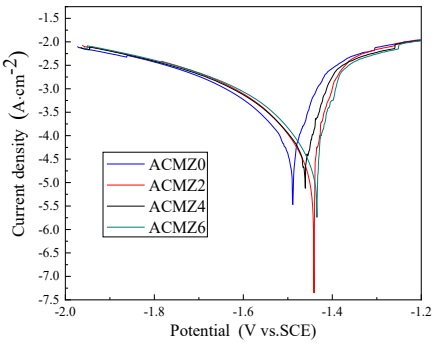


Fig.8. Potentiodynamic polarization curves of as-extruded Mg-1Al-0.3Ca-0.3Mn-based alloys

Table 2 lists the values of Ecorr and icorr obtained from the polarization curves. The ACMZ0 alloy has the most negative corrosion potential and the highest corrosion current density, which indicates that its corrosion resistance is the lowest. With the addition of Zn, the corrosion potential shifts in the positive direction and the corrosion current density decreases, implying that the corrosion resistance is improved. Among the four alloys, the ACMZ2 alloy has the most positive corrosion potential and the lowest corrosion current density, which confirms that it has the best corrosion resistance. The corrosion resistance of the as-extruded alloys therefore follows the order ACMZ0 < ACMZ4 < ACMZ6 < ACMZ2, which is in agreement with the results of the immersion tests.

Table 2 The results of polarization curves of as-extruded Mg-1Al-0.3Ca-0.3Mn-based alloys

Alloys	E_{corr}(V)	I_{corr}(μA•cm^{-2})
ACMZ0	-1.490	71.10
ACMZ2	-1.440	15.40
ACMZ4	-1.460	62.30
ACMZ6	-1.440	29.70

Fig. 9 shows the EIS response of the as-extruded alloys in 3.5 wt.% NaCl solution, and Fig. 10 shows the equivalent circuit used to fit the spectra. In this circuit, Rs is the solution resistance, Rct is the charge-transfer resistance, *RL* and *L* describe the inductive behavior associated with pitting corrosion, and CPE1 is a constant phase element whose impedance is defined as

$$Z_{CPE} = 1 / [Y_0 (j\omega)^n] \quad (2)$$

where Y_o is the admittance of the constant phase element, ω is the angular frequency and n is an empirical exponent that describes the deviation from ideal capacitive behavior ($0 \leqslant n \leqslant 1$). Smaller impedance values were obtained for the ACMZ2 and ACMZ4 electrodes than for the ACMZ0 electrode. Because a smaller diameter of the impedance arc reflects a less protective surface layer, this result suggests that the protective layer on the ACMZ2 and ACMZ4 alloys is the least effective. The fitted parameters are listed in Table 3. The corrosion resistance is governed by

the value of Rct, which reflects the dissolution rate of the α-Mg matrix: a higher Rct corresponds to a better corrosion resistance. The fitted values show that the ACMZ6 alloy has the highest Rct while the ACMZ2 alloy has the lowest, which would imply that the ACMZ2 alloy has the worst corrosion resistance. This ranking is opposite to that obtained from the immersion tests and from the polarization curves; the origin of this apparent inconsistency is discussed in Section 4.4.

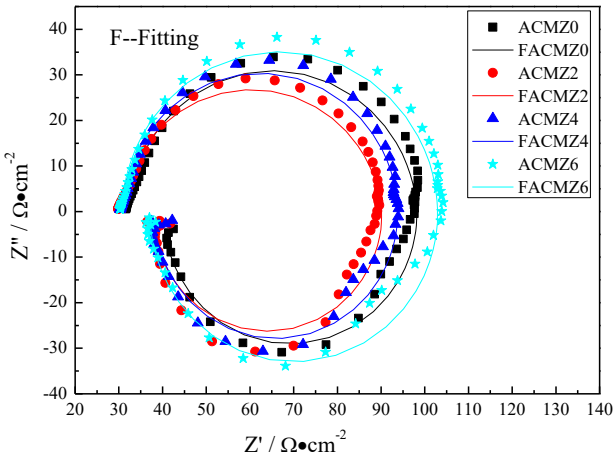


Fig.9. EIS analysis of as-extruded Mg-1Al-0.3Ca-0.3Mn-based alloys in 3.5% saline solution.

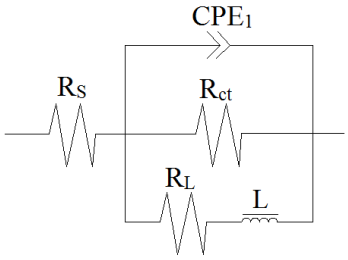


Fig.10. Equivalent circuits of the EIS spectra of as-extruded Mg-1Al-0.3Ca-0.3Mn-based alloys

Table 3 Fitting results of the EIS spectra

Alloys	$R_s(\Omega\cdot cm^2)$	$R_{ct}(\Omega\cdot cm^2)$	$R_L(\Omega\cdot cm^2)$	$L(H\cdot cm^{-2})$	$CPE_1(\Omega^{-1}\cdot s^n\cdot cm^{-2})$
ACMZ0	32.11	66.22	9.216	65.06	$20.34x10^{-6}$
ACMZ2	30.29	60.12	8.603	42.91	$29.23x10^{-6}$
ACMZ4	30.79	63.11	8.298	37.62	$17.78x10^{-6}$
ACMZ6	30.65	72.41	7.066	33.63	$16.27x10^{-6}$

4 Discussion

4.1 Effect of Zn on the microstructure

The XRD results show that the addition of up to 0.6 wt.% Zn does not introduce a new phase: the as-cast alloys contain only α-Mg and Al4Ca, and no Zn-bearing intermetallic is detected. Given that the solid solubility of Zn in α-Mg is much higher than 0.6 wt.% at the temperatures used here, this observation indicates that essentially all of the Zn added in the present study is dissolved in the α-Mg matrix rather than being precipitated as a second phase. This point is important for the interpretation of the corrosion results, because it means that the differences in corrosion behavior

observed between the four alloys cannot be attributed to the presence of a Zn-rich phase acting as an additional cathodic site.

The average grain size of the extruded alloys passes through a minimum at 0.4 wt.% Zn. A first effect of the solute Zn is to modify the kinetics of DRX during extrusion. Solute atoms in solid solution exert a drag force on the moving grain boundaries and on the dislocations, which slows down the migration of the recrystallization front and, at a sufficiently high solute concentration, retards DRX [11]. A low Zn content therefore promotes a more complete recrystallization and a finer recrystallized grain size by providing additional nucleation sites while the boundary mobility remains high enough, whereas a higher Zn content retards DRX and favors the retention of the coarse deformed grains. The appearance of the microstructures in Fig. 2 supports this interpretation: the fraction of coarse elongated grains is smallest for the ACMZ2 and ACMZ4 alloys and largest for the ACMZ0 and ACMZ6 alloys. The increase of the average grain size at 0.6 wt.% Zn is thus consistent with an increasing solute drag effect on the DRX front.

4.2 Effect of Zn on the corrosion behavior

The immersion tests and the polarization curves both show that a small addition of Zn improves the corrosion resistance of the as-extruded Mg–1Al–0.3Ca–0.3Mn alloy, and that the improvement is maximum at 0.2 wt.% Zn. The same ranking is obtained by the two techniques, which is significant because they probe different aspects of the corrosion process: the immersion test measures the cumulative material loss over 168 h, whereas the polarization curve measures the instantaneous kinetics of the anodic and cathodic reactions. The fact that the cathodic branches of the four alloys nearly coincide while their anodic branches differ substantially (Fig. 8) indicates that the Zn addition acts mainly on the anodic dissolution of the matrix rather than on the cathodic reduction of water.

Two features of the results show that the origin of the improvement is not trivial. First, the corrosion-rate sequence ACMZ0 < ACMZ4 < ACMZ6 < ACMZ2 does not correlate with the grain-size sequence, since the ACMZ4 alloy has the finest grains (5.14 μm) but the second highest corrosion rate (3.01×10^{-3} g cm^{-2} h^{-1}). Grain refinement is often invoked to explain an improved corrosion resistance in magnesium alloys, and it has been reported to improve the corrosion resistance of wrought magnesium alloys processed by routes such as double extrusion [28]. Two opposite mechanisms have been proposed in the literature. Aung and Zhou [29] argued that grain boundaries act as physical barriers that slow down the propagation of corrosion from one grain to its neighbor, so that a finer grain size, which provides a higher density of grain boundaries, reduces the corrosion rate. Song and Xu [30] pointed out that grain boundaries are crystal defects that accumulate impurities and solute atoms and can therefore act as cathodic sites that accelerate the dissolution of the adjacent matrix; in that case, grain refinement reduces the amount of impurities and solute atoms segregated in a single grain and weakens the galvanic effect, so that the corrosion resistance again improves. Liu et al. [31] reconciled these views by noting that grain boundaries have a dual effect: they accelerate corrosion when the alloy undergoes anodic dissolution, and they inhibit corrosion when the alloy is able to passivate. Which of the two responses is observed can be shifted by a solute addition, so that localized attack starts either at the grain boundaries or within the grain interiors depending on the alloying element [32]. A recent review of the grain-size

dependence of corrosion emphasizes that the net effect depends on which of these mechanisms dominates in a given system and that the trend is therefore not universal [33,34]. In the present case the grain size of the ACMZ4 alloy is 6% smaller than that of the ACMZ2 alloy, yet its corrosion rate is more than six times higher, and the ACMZ6 alloy has the coarsest grains but a lower corrosion rate than the ACMZ0 and ACMZ4 alloys. Neither of the grain-boundary mechanisms described above can reproduce this sequence, and grain size alone is therefore not the controlling variable. The same conclusion follows from Fig. 1 and Fig. 3, which show that the type, the morphology and the distribution of the second phase are essentially the same in all four alloys.

Because the amount of Zn in solid solution is the only microstructural parameter that varies monotonically over the composition range studied, it is reasonable to attribute the major part of the improvement to the Zn dissolved in the α-Mg matrix. Two effects of the dissolved Zn are consistent with the present observations. The first is the modification of the corrosion-product film. The film that forms on magnesium and on its dilute alloys in chloride media consists mainly of $Mg(OH)_2$, as confirmed by the corrosion products identified after the immersion of Mg–Sn–Ca alloys [35] and of directionally solidified Mg–Zn alloys [36]. This hydroxide is poorly crystalline and only weakly protective, and its protectiveness is sensitive to the presence of divalent cations that can substitute for Mg^{2+} in the hydroxide lattice and change the porosity, the crystallinity and the volume ratio of the film to the metal it replaces [4,37]. The microstructure and the protection characteristics of the naturally formed oxide films on Mg–Zn alloys have been found to depend directly on the Zn content of the alloy [38]. Because Zn^{2+} and Mg^{2+} have similar ionic radii, Zn^{2+} released from the matrix during dissolution can be incorporated into the hydroxide film and make it less permeable to Cl^- ions, which is consistent with the pronounced reduction of the corrosion rate when only 0.2 wt.% Zn is added and with the changes in the anodic branch of the polarization curves. The second effect is a reduction of the effective cathodic area available for micro-galvanic coupling. The Al_4Ca particles are more noble than the α-Mg matrix and therefore act as local cathodes, whereas Mg-rich phases such as Mg_2Ca behave as local anodes in the same matrix [27,39,40]. Because the particles are distributed along the grain boundaries, the extent of this coupling depends on the distribution of the particles with respect to the grain size and on the stability of the surrounding matrix. Reducing the volume fraction of the cathodic phase, or changing its distribution, has been shown to be an effective way of suppressing micro-galvanic corrosion in dilute Mg–Zn–Ca–Mn alloys in 3.5 wt.% NaCl solution [41], and the coupling between grain refinement and the development of a protective corrosion film has been reported to act synergistically in related Mg–Zn–Mn–Ca systems [42]. Any change that makes the matrix more resistant to dissolution, such as the incorporation of Zn into the surface film, reduces the area over which the galvanic couple can operate and therefore lowers the overall corrosion rate. Such micro-alloying strategies, in which a small solute addition alters the growth of the protective film rather than the phase constitution, have been reported to improve the corrosion resistance of magnesium alloys substantially [43].

The fact that 0.6 wt.% Zn is less effective than 0.2 wt.% Zn, although a higher solute content might be expected to strengthen the film further, indicates that the benefit of the dissolved Zn is balanced by a competing effect. The most likely candidate is the coarsening of the microstructure at 0.6 wt.% Zn: the coarser grains of the ACMZ6 alloy provide fewer grain boundaries to act as

barriers to the propagation of corrosion, and they concentrate the Al_4Ca particles in a smaller number of boundaries, which increases the local cathode-to-anode area ratio at those boundaries. The present data do not allow the contribution of the solute Zn to be separated quantitatively from that of the grain size, because the two vary together over the composition range studied, and this separation remains an open question for this alloy system.

4.3 Localized corrosion and pitting

The corrosion of the present alloys is localized rather than uniform. Fig. 5 shows that pitting is the dominant mode of attack in the ACMZ2 alloy at all immersion times, with the pit size increasing from 1–3 μm at 24 h to 10–15 μm at 168 h, and Fig. 6 shows arrays of deep pits on all four alloys after 168 h of immersion. Deep pits have also been reported to form on aluminum-containing magnesium alloys in chloride solutions, where they originate at the interface between the matrix and the intermetallic particles [39,44]. In the present alloys, the Al_4Ca particles at the grain boundaries are the natural initiation sites for pitting, because the potential difference between the particle and the matrix drives the dissolution of the adjacent matrix and produces a local enrichment in Cl^- that prevents the precipitation of a protective hydroxide [27]. Once a pit has been initiated, its interior becomes a preferential site for further dissolution, and the corrosion products that form around the pit mouth do not seal it. The observation that cracks are present on the surface of the ACMZ0 alloy (Fig. 6a and b) but not on the Zn-containing alloys indicates that in the Zn-free alloy the corrosion-product layer not only fails to protect the matrix but also fractures and provides direct pathways for the electrolyte to reach the underlying metal. The thicker and more defective layer on the ACMZ0 alloy is therefore a consequence rather than a cause of its higher corrosion rate, and the beneficial role of Zn is to slow down the processes that lead to the accumulation of this non-protective layer.

4.4 Comparison of the electrochemical and the immersion results

The EIS results rank the four alloys in the opposite order to the immersion tests and the polarization curves, with the ACMZ2 alloy showing the lowest Rct and the ACMZ6 alloy the highest (Table 3). Because this is the only result in the present study that is not internally consistent, its origin requires careful consideration, and several factors that are specific to the way in which the measurements were performed should be taken into account.

First, the EIS spectra were acquired after a stabilization period of only 120 s at the open-circuit potential. Over such a short time the interface that is probed is essentially the freshly prepared, largely film-free surface of the alloy, and the measured response is dominated by the charge-transfer reaction of the matrix and by the adsorption of intermediate species. It is well established for magnesium that the native oxide present on the surface at the moment of immersion, and therefore the impedance measured shortly afterwards, depends strongly on the exposure time before the measurement [45]. The immersion test, in contrast, integrates the corrosion process over 168 h, during which a corrosion-product layer builds up and the interface evolves continuously. Because the matrix composition of the four alloys is nearly identical, with all of the Zn in solid solution and only a small fraction of Al_4Ca present, the short-term charge-transfer response would be expected to be similar for all four alloys, and this is indeed what Table 3 shows: the fitted Rct values (60–72 $\Omega\ cm^2$) differ by less than 20%, which is within the range that is usually attributed

to the scatter of EIS measurements on magnesium alloys. The small spread of the Rct values therefore does not provide a reliable basis for ranking the alloys, and the apparent inversion is more plausibly a reflection of the limited sensitivity of the technique under these conditions than of a genuine reversal of the corrosion resistance.

Second, all four spectra contain a pronounced inductive loop at low frequency, which is described in the equivalent circuit of Fig. 10 by RL and L. The inductive response of magnesium alloys in chloride solutions is generally attributed to the relaxation of adsorbed intermediate species such as Mg^{+} and to the initiation of pitting [46], both of which are processes that are not directly related to the steady-state dissolution rate that the immersion test measures. It should be emphasized, however, that a low-frequency inductive feature in the impedance spectrum of a corroding electrode has several possible physical origins and cannot be assigned to a single mechanism without independent evidence [47]; the interpretation adopted here is therefore provisional. When the inductive contribution is large compared with the capacitive contribution, as it is in the present spectra, the fitted charge-transfer resistance depends strongly on the choice of the equivalent circuit and on the frequency window over which the fit is performed, which further reduces the reliability of a ranking based on Rct alone. It is also worth noting that the fitted spectra in Fig. 9 extend beyond the measured frequency range at high Z', which indicates that the circuit used here does not capture all of the processes that contribute to the response.

Third, the comparison of EIS data with mass-loss data is known to be problematic when the two are acquired on different specimens and at different times. Combined impedance, mass-loss and hydrogen-collection measurements on magnesium have shown that the impedance response correlates with the instantaneous corrosion rate only if the measurement is properly referenced to the evolving surface state, and that a single impedance spectrum is a poor predictor of a long-term corrosion rate [48,49]. A recent review of the use of EIS for magnesium reaches the same conclusion and emphasizes that impedance-derived corrosion rates remain scarce relative to those obtained by mass loss or hydrogen evolution [50]. The same limitation applies to Tafel extrapolation of polarization curves, which for magnesium systematically overestimates the corrosion rate because of the anomalous hydrogen evolution that accompanies anodic dissolution [51]. The impedance of a magnesium electrode in NaCl changes markedly during the first hours of exposure as the surface film develops, so an EIS measurement carried out after 120 s probes a different state of the interface from the one that determines the 168 h corrosion rate. A ranking based on short-term impedance would therefore be expected to differ from a ranking based on long-term mass loss whenever the protectiveness of the film, rather than the intrinsic reactivity of the matrix, controls the corrosion resistance of the alloy—which is precisely the situation that the immersion results indicate for the present alloys.

On the basis of these considerations, the immersion and polarization results, which are mutually consistent and which are based on the actual material loss, are considered to be the more reliable measure of the corrosion resistance of the present alloys. The EIS results are nevertheless valuable because they show that the four alloys have a very similar initial electrochemical response, which supports the interpretation developed in Section 4.2: the differences between the alloys

develop during exposure as a consequence of the interaction between the dissolved Zn and the corrosion-product film, rather than being an intrinsic property of the freshly exposed surfaces.

5 Conclusions

The effects of Zn addition on the microstructure and the corrosion behavior of as-extruded Mg–1Al–0.3Ca–0.3Mn-based alloys were investigated. The following conclusions can be drawn.

(1) The microstructure of the as-extruded Mg–1Al–0.3Ca–0.3Mn-based alloys consists of an α-Mg matrix and Al4Ca particles distributed along the grain boundaries. No Zn-bearing phase is detected over the composition range studied, so that the Zn remains in solid solution. The average grain size decreases from 6.12 μm for the Zn-free alloy to 5.14 μm at 0.4 wt.% Zn and then increases to 7.03 μm at 0.6 wt.% Zn.

(2) According to the immersion tests and the polarization curves, the addition of Zn improves the corrosion resistance of the as-extruded Mg–1Al–0.3Ca–0.3Mn alloy. The corrosion resistance of the as-extruded alloys follows the order ACMZ0 < ACMZ4 < ACMZ6 < ACMZ2, and the alloy containing 0.2 wt.% Zn has the lowest corrosion rate after 168 h of immersion (4.77×10^{-4} g cm^{-2} h^{-1}, only 14.3% of that of the Zn-free alloy).

(3) The corrosion resistance does not correlate with the grain size, because the alloy with the finest grains does not have the lowest corrosion rate. The improvement is therefore attributed mainly to the Zn dissolved in the α-Mg matrix, which modifies the growth of the corrosion-product film and limits the area over which micro-galvanic coupling at the Al_4Ca particles can operate. The beneficial effect reaches a maximum at 0.2 wt.% Zn and is reduced at 0.6 wt.% Zn, where the coarsening of the microstructure counteracts it.

(4) The EIS spectra recorded after 120 s of stabilization rank the four alloys in the opposite order to the immersion tests and the polarization curves. The fitted charge-transfer resistances differ by less than 20% and the spectra contain a pronounced inductive loop, so that this ranking is not considered reliable. The consistency of the immersion and polarization results, which are both based on the actual material loss, indicates that Ecorr, icorr and the mass loss provide the more dependable measure of the corrosion resistance for this alloy system.

Author Contribution All authors have contributed equally to the work, and all authors also read and approved the final manuscript.

Data-availability statement The data that support the findings of this study are available from the corresponding author on reasonable request.

Declarations The authors declare that they have no known competing financial interests or personal relationships that could have appeared to influence the work reported in this paper.

6 References

[1] J.B. Zhang, L.B. Tong, C. Xu, Z.H. Jiang, L.R. Cheng, S. Kamado, H.J. Zhang, Influence of

Ca-Ce/La synergistic alloying on the microstructure and mechanical properties of extruded Mg–Zn alloy, Mater. Sci. Eng. A 708 (2017) 11–20. https://doi.org/10.1016/j.msea.2017.09.113.

[2] Y.L. Lu, Y. Zhang, M.Q. Cong, X.C. Li, W.T. Xu, L.P. Song, Microstructures, mechanical and corrosion properties of the extruded AZ31-xCaO alloys, Materials 11 (2018) 1467. https://doi.org/10.3390/ma11081467.

[3] Y. Zhang, L.P. Song, X.Y. Chen, Y.L. Lu, X.P. Li, Effect of Zn and Ca addition on microstructure and strength at room temperature of as-cast and as-extruded Mg-Sn alloys, Materials 11 (2018) 1490. https://doi.org/10.3390/ma11091490.

[4] M. Esmaily, J.E. Svensson, S. Fajardo, N. Birbilis, G.S. Frankel, S. Virtanen, R. Arrabal, S. Thomas, L.G. Johansson, Fundamentals and advances in magnesium alloy corrosion, Prog. Mater. Sci. 89 (2017) 92–193. https://doi.org/10.1016/j.pmatsci.2017.04.011.

[5] K. Gusieva, C.H.J. Davies, J.R. Scully, N. Birbilis, Corrosion of magnesium alloys: the role of alloying, Int. Mater. Rev. 60 (2015) 169–194. https://doi.org/10.1179/1743280414Y.0000000046.

[6] D.S. Yin, E.L. Zhang, S.Y. Zeng, Effect of Zn on mechanical property and corrosion property of extruded Mg-Zn-Mn alloy, Trans. Nonferrous Met. Soc. China 18 (2008) 763–768. https://doi.org/10.1016/S1003-6326(08)60131-4.

[7] F. Rosalbino, E. Angelini, S. De Negri, A. Saccone, S. Delfino, Effect of erbium addition on the corrosion behaviour of Mg–Al alloys, Intermetallics 13 (2005) 55–60. https://doi.org/10.1016/j.intermet.2004.05.007.

[8] A. Zomorodian, M.P. Garcia, T. Moura e Silva, J.C.S. Fernandes, M.H. Fernandes, M.F. Montemor, Biofunctional composite coating architectures based on polycaprolactone and nanohydroxyapatite for controlled corrosion activity and enhanced biocompatibility of magnesium AZ31 alloy, Mater. Sci. Eng. C 48 (2015) 434–443. https://doi.org/10.1016/j.msec.2014.12.027.

[9] T.T. Sasaki, K. Yamamoto, T. Honma, S. Kamado, K. Hono, A high-strength Mg–Sn–Zn–Al alloy extruded at low temperature, Scr. Mater. 59 (2008) 1111–1114. https://doi.org/10.1016/j.scriptamat.2008.07.042.

[10] Y. Wang, M. Xia, Z. Fan, X. Zhou, G.E. Thompson, The effect of Al8Mn5 intermetallic particles on grain size of as-cast Mg–Al–Zn AZ91D alloy, Intermetallics 18 (2010) 1683–1689. https://doi.org/10.1016/j.intermet.2010.05.004.

[11] T. Homma, S. Hirawatari, H. Sunohara, S. Kamado, Room and elevated temperature mechanical properties in the as-extruded Mg–Al–Ca–Mn alloys, Mater. Sci. Eng. A 539 (2012) 163–169. https://doi.org/10.1016/j.msea.2012.01.074.

[12] C.L. Mendis, K. Oh-ishi, T. Ohkubo, K. Hono, Precipitation of prismatic plates in Mg–0.3Ca alloys with In additions, Scr. Mater. 64 (2011) 137–140. https://doi.org/10.1016/j.scriptamat.2010.09.028.

[13] N. Hort, Y. Huang, D. Fechner, M. Störmer, C. Blawert, F. Witte, C. Vogt, H. Drücker, R.

Willumeit, K.U. Kainer, F. Feyerabend, Magnesium alloys as implant materials – Principles of property design for Mg–RE alloys, Acta Biomater. 6 (2010) 1714–1725. https://doi.org/10.1016/j.actbio.2009.09.010.

[14] H.J. Kim, B.C. Kim, S.M. Baek, S.D. Sohn, H.J. Shin, H.Y. Jeong, C.D. Yim, B.S. You, H.Y. Ha, S.S. Park, Influence of alloyed Al on the microstructure and corrosion properties of extruded Mg–8Sn–1Zn alloys, Corros. Sci. 95 (2015) 133–142. https://doi.org/10.1016/j.corsci.2015.03.007.

[15] S.M. Baek, H.J. Kim, H.Y. Jeong, S.D. Sohn, H.J. Shin, K.J. Choi, K.S. Lee, J.G. Lee, C.D. Yim, B.S. You, H.Y. Ha, S.S. Park, Effect of alloyed Ca on the microstructure and corrosion properties of extruded AZ61 Mg alloy, Corros. Sci. 112 (2016) 44–53. https://doi.org/10.1016/j.corsci.2016.07.011.

[16] S.M. Baek, J.S. Kang, H.J. Shin, C.D. Yim, B.S. You, H.Y. Ha, S.S. Park, Role of alloyed Y in improving the corrosion resistance of extruded Mg–Al–Ca-based alloy, Corros. Sci. 118 (2017) 227–232. https://doi.org/10.1016/j.corsci.2017.01.022.

[17] M. Amirnejad, M. Rajabi, A. Motavalli, Effect of addition of Si on microstructure, mechanical properties, bio-corrosion and cytotoxicity of Mg-6Al-1Zn alloy, Trans. Nonferrous Met. Soc. China 28 (2018) 1755–1762. https://doi.org/10.1016/S1003-6326(18)64819-8.

[18] S.H. Cai, T. Lei, N.F. Li, F.F. Feng, Effects of Zn on microstructure, mechanical properties and corrosion behavior of Mg–Zn alloys, Mater. Sci. Eng. C 32 (2012) 2570–2577. https://doi.org/10.1016/j.msec.2012.07.042.

[19] Y. Yan, H.W. Cao, Y.J. Kang, K. Yu, T. Xiao, J. Luo, Y.W. Deng, H.J. Fang, H.Q. Xiong, Y.L. Dai, Effects of Zn concentration and heat treatment on the microstructure, mechanical properties and corrosion behavior of as-extruded Mg-Zn alloys produced by powder metallurgy, J. Alloys Compd. 693 (2017) 1277–1289. https://doi.org/10.1016/j.jallcom.2016.10.017.

[20] S.X. Zhang, X.N. Zhang, C.L. Zhao, J.N. Li, Y. Song, C.Y. Xie, H.R. Tao, Y. Zhang, Y.H. He, Y. Jiang, Y.J. Bian, Research on an Mg–Zn alloy as a degradable biomaterial, Acta Biomater. 6 (2010) 626–640. https://doi.org/10.1016/j.actbio.2009.06.028.

[21] E.L. Zhang, L. Yang, J.W. Xu, H.N. Chen, Microstructure, mechanical properties and bio-corrosion properties of Mg–Si(–Ca, Zn) alloy for biomedical application, Acta Biomater. 6 (2010) 1756–1762. https://doi.org/10.1016/j.actbio.2009.11.024.

[22] F. Cao, Z. Shi, G.L. Song, M. Liu, A. Atrens, Corrosion behaviour in salt spray and in 3.5% NaCl solution saturated with Mg(OH)2 of as-cast and solution heat-treated binary Mg–X alloys: X = Mn, Sn, Ca, Zn, Al, Zr, Si, Sr, Corros. Sci. 76 (2013) 60–97. https://doi.org/10.1016/j.corsci.2013.06.030.

[23] G.S. Han, D. Chen, G. Chen, J.H. Huang, Development of non-flammable high strength extruded Mg-Al-Ca-Mn alloys with high Ca/Al ratio, J. Mater. Sci. Technol. 34 (2018) 2063–2068. https://doi.org/10.1016/j.jmst.2018.03.019.

[24] M.Z. Bian, T.T. Sasaki, T. Nakata, S. Kamado, K. Hono, Effects of rolling conditions on the

microstructure and mechanical properties in a Mg–Al–Ca–Mn–Zn alloy sheet, Mater. Sci. Eng. A 730 (2018) 147–154. https://doi.org/10.1016/j.msea.2018.05.065.

[25] T. Nakata, C. Xu, R. Ajima, K. Shimizu, S. Hanaki, T.T. Sasaki, L. Ma, K. Hono, S. Kamado, Strong and ductile age-hardening Mg-Al-Ca-Mn alloy that can be extruded as fast as aluminum alloys, Acta Mater. 130 (2017) 261–270. https://doi.org/10.1016/j.actamat.2017.03.046.

[26] B.C. Liu, S. Zhang, H.W. Xiong, W.H. Dai, Y.L. Ma, Effect of Al content on the corrosion behavior of extruded dilute Mg–Al–Ca–Mn alloy, Acta Metall. Sin. (Engl. Lett.) 36 (2023) 77–90. https://doi.org/10.1007/s40195-022-01451-1.

[27] K. Zhang, C. Wang, D.W. Wang, M.X. Li, Y.L. Ma, Z.M. Hua, L.Y. Zhang, J. Li, H.Y. Wang, Effects of solute redistribution during heat treatment on micro-galvanic corrosion behavior of dilute Mg-Al-Ca-Mn alloy, Corros. Sci. 213 (2023) 110971. https://doi.org/10.1016/j.corsci.2023.110971.

[28] X.B. Zhang, Z.Z. Wang, G.Y. Yuan, Y.J. Xue, Improvement of mechanical properties and corrosion resistance of biodegradable Mg–Nd–Zn–Zr alloys by double extrusion, Mater. Sci. Eng. B 177 (2012) 1113–1119. https://doi.org/10.1016/j.mseb.2012.05.020.

[29] N.N. Aung, W. Zhou, Effect of grain size and twins on corrosion behaviour of AZ31B magnesium alloy, Corros. Sci. 52 (2010) 589–594. https://doi.org/10.1016/j.corsci.2009.10.018.

[30] G.L. Song, Z.Q. Xu, The surface, microstructure and corrosion of magnesium alloy AZ31 sheet, Electrochim. Acta 55 (2010) 4148–4161. https://doi.org/10.1016/j.electacta.2010.02.068.

[31] D.X. Liu, C.G. Guo, L.Q. Chai, V.R. Sherman, X.Q. Qin, Y.T. Ding, M.A. Meyers, Mechanical properties and corrosion resistance of hot extruded Mg–2.5Zn–1Ca alloy, Mater. Sci. Eng. B 195 (2015) 50–58. https://doi.org/10.1016/j.mseb.2015.02.001.

[32] Q. Yan, L. Hou, J. Sun, D. Li, J. Song, X. Liu, Q. Wang, Y. Wei, Regulating the localized corrosion of grain boundary and galvanic corrosion by adding the electronegative element in magnesium alloy, Corros. Sci. 244 (2025) 112667. https://doi.org/10.1016/j.corsci.2024.112667.

[33] K.D. Ralston, N. Birbilis, Effect of grain size on corrosion: a review, Corrosion 66 (2010) 075005. https://doi.org/10.5006/1.3462912.

[34] A. Bahmani, M. Lotfpour, M. Taghizadeh, W.J. Kim, Corrosion behavior of severely plastically deformed Mg and Mg alloys, J. Magnes. Alloys 10 (2022) 2607–2648. https://doi.org/10.1016/j.jma.2022.09.007.

[35] C.Y. Zhao, F.S. Pan, H.C. Pan, Microstructure, mechanical and bio-corrosion properties of as-extruded Mg–Sn–Ca alloys, Trans. Nonferrous Met. Soc. China 26 (2016) 1574–1582. https://doi.org/10.1016/S1003-6326(16)64232-2.

[36] H.M. Jia, X.H. Feng, Y.S. Yang, Microstructure and corrosion resistance of directionally solidified Mg-2 wt.% Zn alloy, Corros. Sci. 120 (2017) 75–81.

https://doi.org/10.1016/j.corsci.2017.02.023.
[37] Y.J. Li, M.X. Li, B.Y. Wang, M.W. Ren, C. Wang, M. Zha, Y. Gao, H.Y. Wang, Effect of Sn addition on the microstructure and corrosion behavior of dilute wrought Mg-Zn-Ca series alloys, Corros. Sci. 235 (2024) 112180. https://doi.org/10.1016/j.corsci.2024.112180.
[38] Y. Song, E.H. Han, K. Dong, D. Shan, C.D. Yim, B.S. You, Microstructure and protection characteristics of the naturally formed oxide films on Mg–xZn alloys, Corros. Sci. 72 (2013) 133–143. https://doi.org/10.1016/j.corsci.2013.03.021.
[39] C. Zhang, L. Wu, G. Huang, Y. Huang, B. Jiang, A. Atrens, F. Pan, Effect of microalloyed Ca on the microstructure and corrosion behavior of extruded Mg alloy AZ31, J. Alloys Compd. 823 (2020) 153844. https://doi.org/10.1016/j.jallcom.2020.153844.
[40] P. Yang, S. Ye, B. Feng, J. Liu, S. Huang, G. Liu, W. Zhang, W. Tang, S. Zhu, S. Zhang, Microgalvanic corrosion of Mg–Ca and Mg–Al–Ca alloys in NaCl and Na2SO4 solutions, Materials 14 (2021) 7140. https://doi.org/10.3390/ma14237140.
[41] Y.Z. Wang, L.X. Chen, B.Q. Shi, H. Yan, R.S. Chen, Enhancing the corrosion resistance of dilute Mg–Zn–Ca–Mn alloys by alleviating micro-galvanic corrosion via tailoring the secondary phases, J. Mater. Res. Technol. 38 (2025) 2675–2689. https://doi.org/10.1016/j.jmrt.2025.08.102.
[42] S. Sha, F. Wang, R.G. Li, X.P. Li, H. Zhang, B.S. Liu, S.S. Li, Y. Tang, High-strength corrosion-resistant and degradable Mg-Zn-Mn-Ca alloy: dynamic precipitation-induced grain refinement and corrosion film synergistic strengthening, J. Alloys Compd. 1039 (2025) 183410. https://doi.org/10.1016/j.jallcom.2025.183410.
[43] M. Deng, L. Wang, D. Höche, S.V. Lamaka, C. Wang, D. Snihirova, Y. Jin, Y. Zhang, M.L. Zheludkevich, Approaching “stainless magnesium” by Ca micro-alloying, Mater. Horiz. 8 (2021) 589–596. https://doi.org/10.1039/D0MH01380C.
[44] Y. Liu, W.L. Cheng, Y.H. Liu, X.F. Niu, H.X. Wang, L.F. Wang, Z.Q. Cui, Effect of alloyed Ca on the microstructure and corrosion behavior of extruded Mg-Bi-Al-based alloys, Mater. Charact. 163 (2020) 110292. https://doi.org/10.1016/j.matchar.2020.110292.
[45] M. Felten, J. Nowak, O. Beyss, P. Grünewald, C. Motz, D. Zander, The effect of time dependent native oxide surface conditions on the electrochemical corrosion resistance of Mg and Mg-Al-Ca alloys, Corros. Sci. 212 (2023) 110925. https://doi.org/10.1016/j.corsci.2022.110925.
[46] M.P. Gomes, I. Costa, N. Pébère, J.L. Rossi, B. Tribollet, V. Vivier, On the corrosion mechanism of Mg investigated by electrochemical impedance spectroscopy, Electrochim. Acta 306 (2019) 61–70. https://doi.org/10.1016/j.electacta.2019.03.080.
[47] D. Klotz, Negative capacitance or inductive loop? – A general assessment of a common low frequency impedance feature, Electrochem. Commun. 98 (2019) 58–62. https://doi.org/10.1016/j.elecom.2018.11.017.
[48] A.D. King, N. Birbilis, J.R. Scully, Accurate electrochemical measurement of magnesium corrosion rates; a combined impedance, mass-loss and hydrogen collection study, Electrochim.

Acta 121 (2014) 394–406. https://doi.org/10.1016/j.electacta.2013.12.124.
[49] M. Curioni, F. Scenini, T. Monetta, F. Bellucci, Correlation between electrochemical impedance measurements and corrosion rate of magnesium investigated by real-time hydrogen measurement and optical imaging, Electrochim. Acta 166 (2015) 372–384. https://doi.org/10.1016/j.electacta.2015.03.050.
[50] S. Feliu, Electrochemical impedance spectroscopy for the measurement of the corrosion rate of magnesium alloys: brief review and challenges, Metals 10 (2020) 775. https://doi.org/10.3390/met10060775.
[51] Z. Shi, M. Liu, A. Atrens, Measurement of the corrosion rate of magnesium alloys using Tafel extrapolation, Corros. Sci. 52 (2010) 579–588. https://doi.org/10.1016/j.corsci.2009.10.016.